Experimental Characterisation: Rich Deformations

Cormac Flynn

Abstract Human skin is a complex material that exhibits a non-linear stress-strain response, anisotropy, and viscoelasticity. In addition, skin in vivo is under an anisotropic pre-stress, which varies according to location and person. While several methods have been developed to measure the in vivo mechanical response of skin, many of these are incapable of characterising the anisotropy. Few also attempt to measure the in vivo stress. To quantify the anisotropy, it is necessary to apply deformations to the skin in a number of directions. This chapter provides an overview of a method where a rich set of deformations are applied to the surface of the skin and the nonlinear, anisotropic, and viscoelastic response is characterised using finite element analyses and nonlinear optimisation. The in vivo stress is also estimated. Different constitutive models were tested as to their suitability to represent skin. Material parameters and pre-stresses were identified for points on the anterior forearm, upper arm, and the face.

1 Introduction

The mechanical characterisation of human skin is driven by its application in a broad range of disciplines. Better knowledge of skin properties would lead to improved identification and treatment of certain diseases [7, 20, 26]. The development of consumer products, such as razors, sanitary pads, nappies, and sticking plasters would benefit from better mechanical knowledge of the skin they are in contact with [8, 24, 42]. More recently, wearable sensors and trans-dermal patches are required to adhere to, stretch and deform with the skin they are attached to for long periods [22, 28]. Characterisation of facial skin is particularly important for the development of realistic computational social agents [37] and social-care robots [25]. A challenge for both these fields is the development of facial models that cross the 'uncanny

C. Flynn (✉)
Galway-Mayo Institute of Technology, Galway, Ireland
e-mail: cormac.flynn@gmit.ie

G. Limbert (ed.), *Skin Biophysics*, Studies in Mechanobiology,
Tissue Engineering and Biomaterials 22,
https://doi.org/10.1007/978-3-030-13279-8_7

valley'—a phenomenon that proposes the more realistic artificial faces become the more eerie and repulsive to a perceiver they are [31].

There are many studies in the literature that characterise some aspects of the mechanical response of skin. The approaches taken are manifold including applying suction, normal indentation, torsion, in-plane shear, uniaxial and biaxial tension to the skin surface. Several of these methods, including suction and normal indentation are unable to characterise the anisotropic nature of skin due to their axisymmetrical loading. To capture the multi-directional properties of skin, it is necessary to apply deformations to the skin in a number of directions.

Reihsner et al. [36] derived elastic constants for in vitro skin samples by stretching them in-plane in a multi-axial tester. The six elastic constants were determined for each of the 16 skin sites sampled. Jor et al. [23] estimated the material parameters for a structural model of porcine skin by a combination of multi-axial in vitro stretching and digital image correlation (DIC). Affagard et al. [1] proposed an experimental protocol to improve the identification of material parameters for a single skin assay ex vivo. The protocol included uniaxial loading, equibiaxial loading, and alternated biaxial loading all combined with DIC. DIC combined with bulge tests have been recently used to characterise the anisotropic mechanical properties of ex vivo human skin [41].

While in vitro or ex vivo tests are valuable in determining detailed relationships between microstructure and mechanical response, it is of interest to characterise the skin in vivo. For instance, a clinician may want to measure the mechanical response of a patient's skin to track the progression of disease such as lymphoedema. Kvistedal and Nielsen [27] used a similar experimental set up as Jor et al. [23] to characterise in vivo forearm skin of several volunteers. They used nonlinear optimisation techniques to estimate the material parameters that best fit the Tong and Fung [40] model to each volunteer's skin. This protocol included attaching the skin to 16 pads, each of which were attached to an actuator. It is the opinion of the author that this protocol would be difficult and time consuming to use in the clinical setting.

Coutts et al. [7] used a uniaxial extensometer in two directions to characterise the in vivo skin anisotropy in breast cancer related lymphoedema. More recently, Then et al. [39] used an extensometer device in multiple directions to characterise the in vivo response of facial skin. The use of an extensometer has the disadvantage of having to reconfigure the apparatus for each direction. The reconfiguration introduces a delay in the acquisition of the data and uncertainty of the position at the skin site. Evans and Holt [11] pulled a wire attached to in vivo forearm skin in different directions and tracked the displacements using digital image correlation. Optimisation using a finite element model estimated Ogden material parameters and the in vivo strain. Multi-view stereo techniques have also been used to track deformations and growth of living skin [38]. These approaches have the distinct advantage of not having to reconfigure the instrumentation to measure the response in different directions.

This chapter presents an approach to characterise in vivo human skin using a micro-robotic device. Firstly, details of the force-sensitive micro-robot are pre-

sented. Secondly, the protocols for applying a rich set of deformations to areas of the arm and face are detailed. Thirdly, the constitutive models, finite element model, and non-linear optimisation techniques used to identify material parameters and in vivo stresses are introduced. Results from these experiments are detailed. Lastly, current challenges in determining the mechanical properties of in vivo human skin are discussed and future opportunities are identified.

2 Multi-Directional Characterisation of Skin Using a Micro-Robotic Device

This section presents details of the force-sensitive micro-robot and how it is used to measure the force-displacement response of different points on the face and arm. The finite element model used to simulate the experiments is introduced along with the constitutive models used to represent the skin. The section concludes with the non-linear optimisation procedure to identify model parameters.

2.1 Method or Applications

2.1.1 Force-Sensitive Micro-Robot

The micro-robot consisted of three parallel axes, which were driven by voice-coil actuators (BEI KIMCO LA10-12-027A) Fig. 1. These moved a platform in three-dimensional space. The axes were guided by precison linear slides (IKO BSP 730SL). On top of each axis there was a vee-jewel bearing. Inside each bearing sat a steel pivot, which was connected to the platform via a linear slide. Small springs prevented the steel pivots from lifting out of the bearings.

Three force-transducers (FSS1500NC, Honeywell, Freeport, IL, USA) were fixed to the moving platform at the apices of a 15-mm equilateral triangle. The legs of a rigid frame sat upon each force transducer. Two neodymium magnets on the frame and platform kept the frame in place on the force transducers.

On the tip of the frame sat a 4-mm-diameter cylindrical probe. The force acting on the probe was determined from the measured forces acting on the force transducers according to the relation:

$$\begin{bmatrix} R_X \\ R_Y \\ R_Z \end{bmatrix} = \begin{pmatrix} -\sqrt{3}w/2h & 0 & \sqrt{3}w/2h \\ -w/2h & w/h & -w/2h \\ -1 & -1 & -1 \end{pmatrix} \begin{bmatrix} F_X \\ F_Y \\ F_Z \end{bmatrix} \tag{1}$$

where R_X, R_Y, R_Z are the components of the probe tip reaction force. F_A, F_B, F_C are the measured forces, w is the distance from the centroid to an apex of the triangle

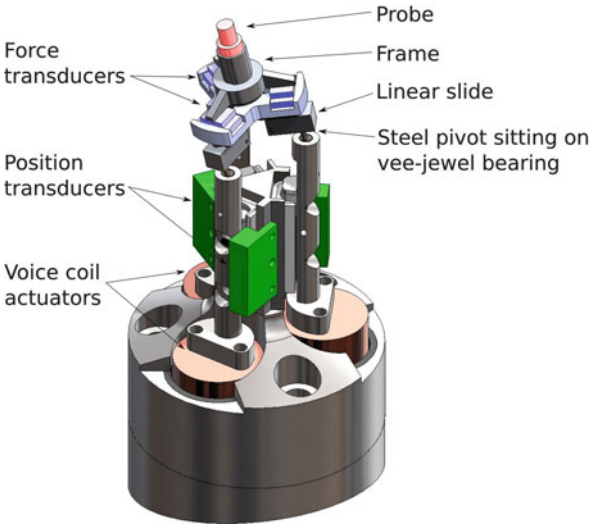

Fig. 1 Force-sensitive micro-robot. Reprinted by permission from Springer: Computer Methods in Biomechanics and Biomedical Engineering. Lecture Notes in Bioengineering, Gefen A., Weihs D., 2018

formed by the three force transducers, and h is the perpendicular distance between the probe tip and the base of the rigid frame.

Linear position transducers (RDC1014, ALPS, Campbell, CA, USA) measured the displacements of the parallel axes. Using a forward kinematics algorithm, the displacement of the probe tip was calculated. A LabView software interface (National Instruments, Austin, USA) controlled the motion of the probe and recorded the position and force data. Axes position feedback signals provide closed-loop position control. The integrated PID controller on the motion control card (NI 7358, National Instruments, Austin, USA) was used. The resolution of the probe tip displacement was 50 μm and the resolution of the measured force was 6 mN.

2.1.2 In vivo Experiments

The micro-robot applied a rich-set of deformations and measured the force response of different skin areas of the arms and faces of volunteers. On the right arm, areas on the posterior upper arm and anterior forearm were tested (Fig. 2a). On the face, six areas were tested: the centre of the right-hand cheek, the centre of the right-hand jaw, on the right-hand cheek near the lips, the right-hand parotideomasseteric region, the right-hand zygomatic region, and the centre of the forehead (Fig. 2b).

For each test, the relevant area of the face or arm was rested on a support plate positioned above the probe of the micro-robot. A hole in the support-plate allowed the probe to be attached to the skin using cyanoacrylate adhesive. A visual inspection after the tests indicated that the probe remained fixed to the surface of the skin throughout. For the arm experiments, double-sided tape was placed around the edge of the whole. As a result, skin in contact with the support plate did not move.

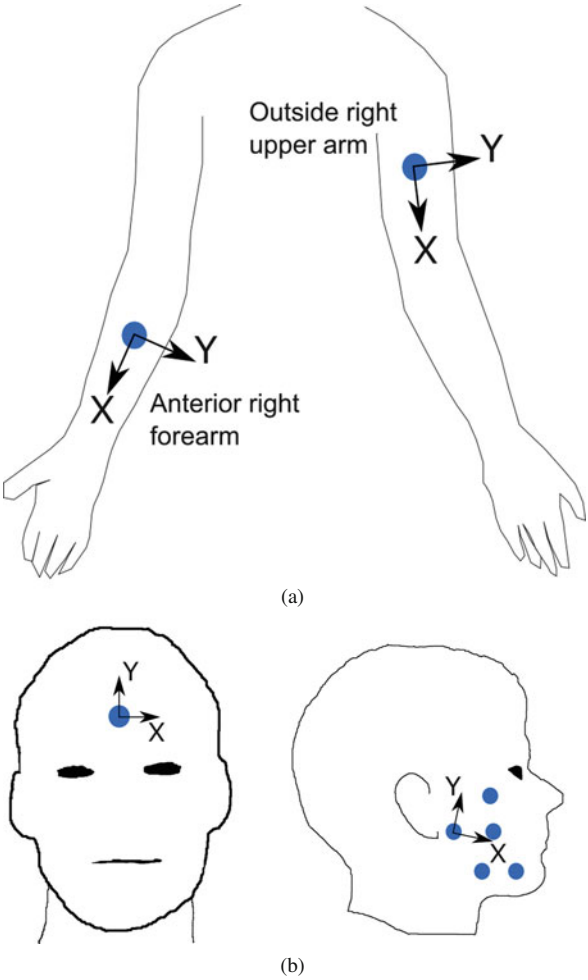

Fig. 2 Locations where the micro-robot probe was attached. (**a**) Arm locations; (**b**) face locations. X and Y axes indicate probe displacement coordinate axes (see Fig. 4). The orientation of the axes is the same for all locations on the face. Reprinted by permission from Springer: Computer Methods in Biomechanics and Biomedical Engineering. Lecture Notes in Bioengineering, Gefen A., Weihs D., 2018

This was verified through visual inspection. This provided a boundary condition for the finite element analyses described later. For the facial skin experiments, a boundary ring was attached using double-sided tape to the volunteer's face, centring it on the region of interest. The boundary ring slotted into a corresponding hole on the support plate in only one orientation. This ensured that the orientation of the face with respect to the micro-robot was known. Similar to the arm experiments, facial skin in contact with the boundary ring and support plate did not move (Fig. 3).

For all skin areas tested, the attached probe moved according to a rich set of deformations. For each direction, the probe moved according to three triangular wave cycles of frequency 0.1 Hz. Three cycles were used to precondition the skin. This was done to get a consistent skin response. It was found that the skin was pre-conditioned after one cycle. The probe was first moved in the plane of the skin

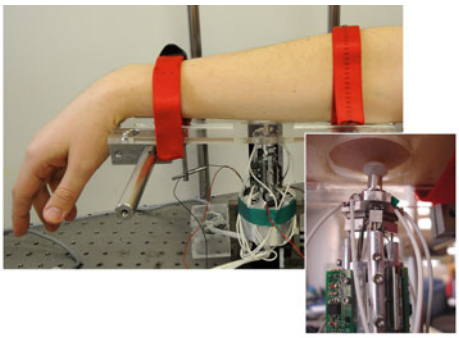

(a)

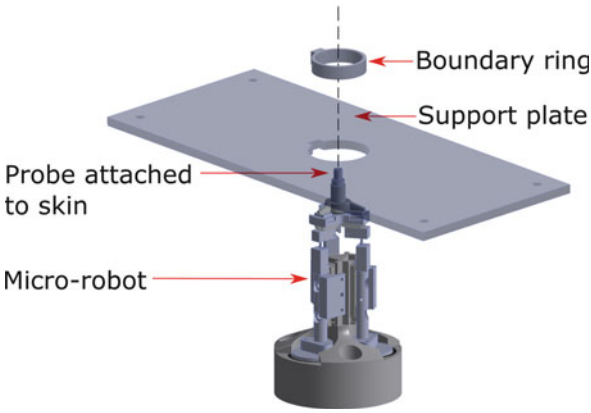

(b)

Fig. 3 Experimental set-up. (**a**) Arm experiments; (**b**) for the facial skin experiments, the boundary ring is attached to the volunteer's face and centred at one of the locations indicated in Fig. 2b. Reprinted by permission from Springer: Computer Methods in Biomechanics and Biomedical Engineering. Lecture Notes in Bioengineering, Gefen A., Weihs D., 2018

surface in a direction $\theta = 0°$ (Fig. 4). The amplitude of the displacement was approximately 1.2–1.4 mm depending on the local stiffness of the skin. The angle of the displacement was then increased in steps of 10°, 20°, or 30° up to $\theta = 180°$ for the arm locations and $\theta = 330°$ for the facial locations. Next a series of out-of-plane displacements were applied to the areas of interest, where $\theta = 0°$, 45°, and 90°, and $\phi = 45°$. The final displacement was in a direction normal to and away from the surface of the skin ($\theta = 0°, \phi = 90°$). There was no wait time between each direction.

The time, probe displacement, and probe reaction force was recorded for all tests on the arms and faces.

2.1.3 Finite Element Models

Finite element models simulated the in vivo arm and facial skin experiments. Different packages were used in the various studies. ABAQUS Version 6.7 (SIMULIA,

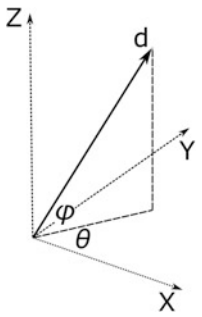

Fig. 4 The probe was displaced in different in-plane and out-of-plane directions. For the arm skin there were in-plane directions with $\theta = 0°, 30° \ldots 180°$ and $\phi = 0°$. For facial skin there were 12 in-plane directions with $\theta = 0°, 30° \ldots 330°$ and $\phi = 0°$. For all regions, there were three out-of-plane directions with $\theta = 0°, 45°, 90°$ and $\phi = 45°$, and one normal direction with $\theta = 0°$ and $\phi = 90°$. $d \approx 1.2$–1.4 mm for all directions. See Fig. 2 for orientation of axes at the arm and face locations. Reprinted by permission from Springer: Computer Methods in Biomechanics and Biomedical Engineering. Lecture Notes in Bioengineering, Gefen A., Weihs D., 2018

Providence, RI) was used for the arm studies, and ANSYS (Canonsburg, PA, USA) and FEBio [30] were used for the face studies. Different packages were used according to their availability in the institutes where the studies were conducted. There were some differences in the models due to functional differences between the packages. For example, the *INITIAL CONDITIONS keyword in ABAQUS allowed us to define a stress field in the reference configuration. This facility was not available in the other packages. The model for the facial skin study in Flynn et al. [14] is described here.

A square domain of side 50 mm represented the skin (Fig. 5). The inside edge of the hole in the support plate and the outside edge of the probe were represented by two circular partitions. The domain was meshed using 2432 quadrilateral shell elements of thickness 1.5 mm, which is representative of the thickness of skin in the relevant areas of the face and arm [18, 36]. Underlying layers of skin were ignored in this model. The implications of this assumption are addressed in the conclusions.

Two static analysis steps were performed. The first step applied a pre-stress to the skin. All four edges were fixed in the Z direction. Boundary conditions were applied to two adjacent edges such that they only shortened along their length when the domain was stretched (Fig. 5). Loads were applied normal to the edge of the opposite sides. The loads were linearly ramped from zero to the full load in 5 s. The magnitude of the loads varied according to the location on the body and were determined through the non-linear optimisation procedure described later. As it was assumed the skin outside the hole in the support plate did not move in the experiments, in the second static analysis step all nodes outside the larger circular partition were fixed in all degrees of freedom. The nodes inside the smaller circular partition were displaced according to the displacement of the probe in the

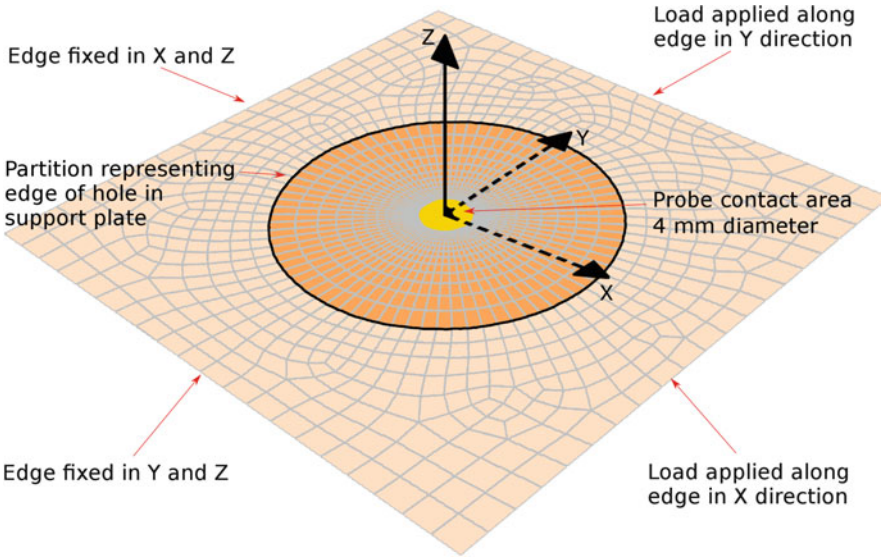

Fig. 5 Finite element model of the in vivo experiments. Reprinted by permission from Springer: Computer Methods in Biomechanics and Biomedical Engineering. Lecture Notes in Bioengineering, Gefen A., Weihs D., 2018

experiments. The magnitude and direction of the sum of the reaction forces within the probe region were calculated at each step.

2.1.4 Constitutive Models

For both arm and facial skin studies, several constitutive models were tested as to their suitability in representing skin. The models are briefly described here.

For the arm studies, the Ogden [32] model and the Tong and Fung [40] model were used to represent the skin. For the facial skin studies, in addition to the Ogden model, the Bischoff et al. [4] model, a frame invariant version of the Fung constitutive equation [2], and the Gasser et al. [17] model were tested as to their suitability to represent skin.

The Ogden [32] model was used to both represent arm and facial skin. Using this isotropic model with an anisotropic pre-stress field can capture the anisotropic response of skin in a manner similar to Bischoff et al. [3].

$$W_{\text{Ogden}} = \sum_{i=1}^{2} \frac{\mu_i}{\alpha_i} \left(\lambda_1^{\alpha_i} + \lambda_2^{\alpha_i} + \lambda_3^{\alpha_i} \right) + U(J) \tag{2}$$

where μ_i, and α_i are material parameters.

The volumetric component of the strain energy function is

$$U(J) = \frac{B}{2}(\ln J)^2 \tag{3}$$

where $B = 1$ MPa is the bulk modulus representing the near incompressibility of skin and $J = det\mathbf{F}$ is the volume ratio. $\mathbf{F}$ is the deformation gradient.

The anisotropic Tong and Fung [40] model was used to represent arm skin.

$$W_{\text{Tong}} = \alpha_1 E_{11}^2 + \alpha_2 E_{22}^2 + \alpha_3 E_{11} E_{22} + c e^{A_1 E_{11}^2 + A_2 E_{22}^2} + U(J) \tag{4}$$

where E_{11} and E_{22} are components of the Lagrangian strain tensor and α_1, α_2, α_3, c, A_1, and A_2 are material parameters. α_1, α_2, α_3, and c control the stiffness at low strains, while A_1, and A_2 control the stiffness of the response at high strains.

The Bischoff et al. [4] model was used to represent facial skin and was implemented into FEBio using the user material plug-in facility.

$$W_{\text{Bischoff}} = \frac{nk\theta}{4}\left(P^2 \sum_{i=1}^{4}\left[\frac{\rho^{(i)}}{P^2}\beta_\rho^{(i)} + \ln\frac{\beta_\rho^{(i)}}{\sinh\beta_\rho^{(i)}}\right] - \frac{\beta_P}{P}\ln\left[\bar{\lambda}_{\mathbf{a}}^{a^2}\bar{\lambda}_{\mathbf{b}}^{b^2}\bar{\lambda}_{\mathbf{c}}^{c^2}\right]\right) + U(J) \tag{5}$$

where a, b, and c are the lengths of a cell, n is the number of fibres per unit volume, $k = 1.38 \times 10^{-23}\,\text{JK}^{-1}$ is Boltzman's constant, and θ is the absolute temperature.

$\bar{\lambda}_{\mathbf{a}} = \sqrt{\mathbf{a}^T\bar{\mathbf{C}}\mathbf{a}}$, $\bar{\lambda}_{\mathbf{b}} = \sqrt{\mathbf{b}^T\bar{\mathbf{C}}\mathbf{b}}$, $\bar{\lambda}_{\mathbf{c}} = \sqrt{\mathbf{c}^T\bar{\mathbf{C}}\mathbf{c}}$ are the principal fibre stretches along the principal material axes of the cell, $(\mathbf{a}, \mathbf{b}, \mathbf{c})$. $\bar{\mathbf{C}}$ is the deviatoric right Cauchy tensor.

$P = \frac{1}{2}\sqrt{a^2 + b^2 + c^2}$ is the undeformed length of a fibre in the cell, while $\rho^{(i)}$ is the deformed length of the i^{th} fibre. $\beta_\rho^{(i)} = \mathscr{L}^{-1}\left(\frac{\rho^{(i)}}{N}\right)$, with $\mathscr{L}(x) = \coth x - \frac{1}{x}$ being the Langevin function.

A frame invariant version of the Fung constitutive equation proposed by Ateshian and Costa [2] was also tested for facial skin.

$$W_{\text{Fung}} = \frac{c}{2}(\mathrm{e}^Q - 1) + U(J) \tag{6}$$

$$Q = c^{-1}\sum_{a=1}^{3}\left[2\mu_a\mathbf{a}_a^0 \otimes \mathbf{a}_a^0 : \bar{\mathbf{E}}^2 + \sum_{b=1}^{3}\lambda_{ab}(\mathbf{a}_a^0 \otimes \mathbf{a}_a^0 : \bar{\mathbf{E}})(\mathbf{a}_b^0 \otimes \mathbf{a}_b^0 : \bar{\mathbf{E}})\right] \tag{7}$$

where c is a parameter representing the stiffness, and λ_{ab}, μ_a are Lamé parameters. All parameters have units of stress. $\bar{\mathbf{E}} = \frac{1}{2}(\bar{\mathbf{F}}^T\bar{\mathbf{F}} - \mathbf{I})$ is the deviatoric Green-Lagrange strain tensor. $\mathbf{a}_a^0$ defines an initial direction of a material axis a, which is prescribed in the X direction (Fig. 5). For the purposes of simplifying the parameter optimisation procedure, $\lambda_{11} = \lambda_{12} = \lambda_{23} = \lambda_{31}$, $\lambda_{22} = \lambda_{33}$, and $\mu_2 = \mu_3$.

An anisotropic model proposed by Gasser et al. [17] was the fourth model used for facial skin.

$$W_{\text{Gasser}} = \frac{\mu}{2}(\bar{I}_1 - 1) + \frac{k_1}{k_2}\{e^{k_2[\tilde{I}_n(\theta)-1]^2} - 1\} + U(J) \tag{8}$$

where μ, k_1 control the stiffness of the skin at small strains and k_2 is a dimensionless parameter that controls the stiffness at large strains. $\tilde{I}_n(\theta) = \mathbf{N}\bar{\mathbf{C}}\mathbf{N}$ is the fibre stretch squared of the n^{th} family of fibres orientated in the direction $\mathbf{N}$ in the reference configuration.

In all the studies, a quasi-linear viscoelastic model proposed by Fung [15] characterised the time-dependent properties of skin.

$$\mathbf{T}(t) = \mathbf{T}_e(t) + \int_0^t \mathbf{T}_e(t-\tau)\frac{\partial g_R(\tau)}{\partial \tau}\,\mathrm{d}\tau, \tag{9}$$

where $\mathbf{T}(t)$ is the total Cauchy stress at time t, $\mathbf{T}_e = \frac{1}{J}\mathbf{F}\frac{\partial W}{\partial E}\mathbf{F}^T$ is the elastic Cauchy stress, and $g_R(t)$ is a Prony series relaxation function.

$$g_R(t) = 1 - \bar{g}_1^P(1 - e^{-t/\tau_1^G}) \tag{10}$$

where $\bar{g}_1^P = 0.4$ is a viscoelastic parameter and $\tau_1^G = 0.8\,\text{s}$ is the relaxation time. The same Prony parameters were used for all locations. The values were chosen such that the hysteresis level in the model matched the hysteresis level measured in the experiments.

2.1.5 Framework for Identification of Model Parameters

Constitutive material parameters and the pre-stress field that best fit the model probe reaction forces to the measured probe reaction forces from the in vivo experiments were determined. The optimisation procedure used the lsqnonlin function in MATLAB 2016a (The Mathworks, Inc., Natwick, MA, USA). This function minimised the following objective function in a least squares sense using a trust region method

$$F(\mathbf{x}) = \sum_{i=1}^{16}\sum_{j=1}^{N_i}\left\{\left(\frac{R_{X_j}^{model}(\mathbf{x}) - R_{X_j}^{exp}}{max\left(R_{X_j}^{exp}\right)}\right)^2 + \left(\frac{R_{Y_j}^{model}(\mathbf{x}) - R_{Y_j}^{exp}}{max\left(R_{Y_j}^{exp}\right)}\right)^2 + \left(\frac{R_{Z_j}^{model}(\mathbf{x}) - R_{Z_j}^{exp}}{max\left(R_{Z_j}^{exp}\right)}\right)^2\right\} \tag{11}$$

where $\mathbf{x}$ is the model parameter set, and N_i is the number of data points recorded for the i^{th} probe direction (16 directions for the face experiments and 8 directions for the arm experiments). $R_{X_j}^{model}(\mathbf{x})$, $R_{Y_j}^{model}(\mathbf{x})$, and $R_{Z_j}^{model}(\mathbf{x})$ are the model probe reaction forces in the X, Y, and Z directions at the j^{th} data point. $R_{X_j}^{exp}$, $R_{Y_j}^{exp}$, $R_{Z_j}^{exp}$ are the experiment probe reaction forces in the X, Y, and Z directions at the j^{th} data point. A customised MATLAB script assembled the input files for the finite element analyses. Upon completion of the analyses, the results were read and the objective function in Eq. (11) was calculated. The lsqnonlin function adjusted the material parameters and pre-loads and updates the input files for another round of finite element analyses. This iterative procedure continued until a local minimum in the objective function was found. Parameter sets were identified that fit the model data to the in vivo data for different points on the arm and face. The variance accounted for (VAF) was calculated for each set.

$$VAF = 1 - \frac{F(\mathbf{x})}{\sum_{i=1}^{16}\sum_{j=1}^{N_i}\left\{\left(\frac{R_{X_j}^{exp}}{max\left(R_{X_j}^{exp}\right)}\right)^2 + \left(\frac{R_{Y_j}^{exp}}{max\left(R_{Y_j}^{exp}\right)}\right)^2 + \left(\frac{R_{Z_j}^{exp}}{max\left(R_{Z_j}^{exp}\right)}\right)^2\right\}} \tag{12}$$

2.2 Results

For both the arm and face experiments, the mechanical response of the skin was nonlinear, anisotropic, and viscoelastic (sample results shown in Figs. 6 and 7). The experimental method demonstrated good repeatability with force-displacement responses from multiple tests on the cheek of one volunteer differing by less than 10%.

There were notable differences in the stiffness of the response between volunteers. The anisotropy of the skin of volunteers was similar. In general, the directions of the stiffest responses for all tested locations between volunteers were the same (Fig. 8). The stiffest response on the forearm was along the length of the arm, while for the upper arm the stiffest response was approximately perpendicular to the longitudinal axis of the arm. For the central cheek area, the stiffest response was approximately in the X direction indicated in Fig. 3b.

All six facial locations exhibited anisotropic characteristics (Fig. 9). For the central cheek, central jaw, near ear, and zygomatic regions, the in-plane force-displacement response was stiffest approximately along the 150–330° axis and least stiff approximately along the 60–240° axis. At the near lip and forehead locations, the in-plane responses were stiffest along the 0–180° axis and least stiff along the 90–270° axis.

The Ogden [32] model simulated the response of the anterior forearm with VAFs ranging from 98% to 99% (table 1). The Tong and Fung [40] model simulated the

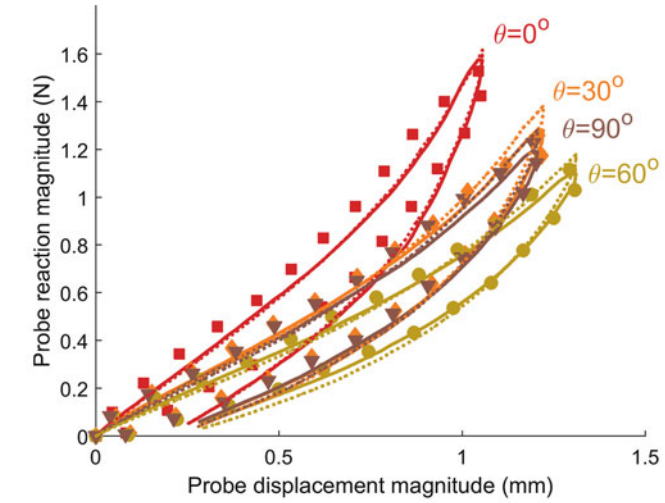

(a)

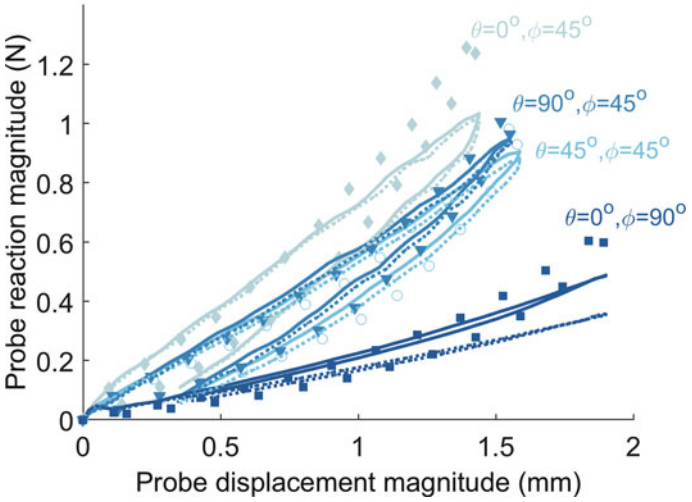

(b)

Fig. 6 Experimental and model force-displacement response for the stiffest anterior forearm skin. (**a**) In-plane response; (**b**) out-of-plane response. Experimental data indicated by symbols; Tong and Fung [40] model indicated by solid lines; Ogden [32] model indicated by dashed lines. See Table 1 for model parameters and pre-stresses. Reprinted by permission from Springer: Annals of Biomedical Engineering, Modeling the Mechanical Response of In Vivo Human Skin Under a Rich Set of Deformations, Cormac Flynn, Andrew Taberner, and Poul Nielsen, 2011

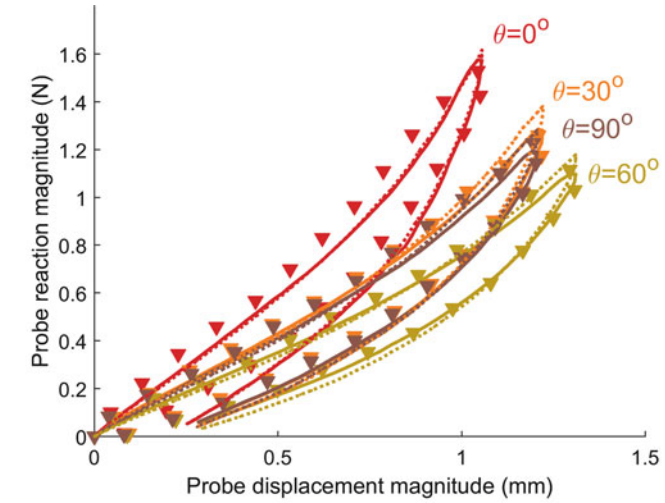

(a)

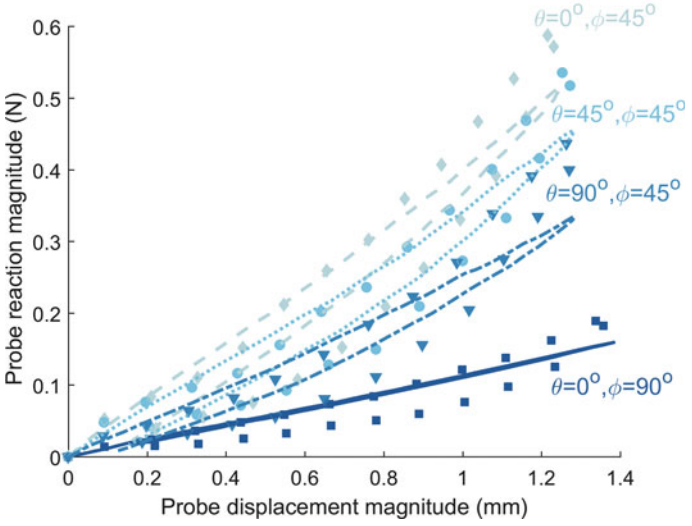

(b)

Fig. 7 Experiment and Bischoff et al. [4] model probe reaction-displacement response for forehead region. (**a**) In-plane response; (**b**) out-of-plane response. *VAF* for Bischoff et al. [4] was 94%. See Table 2 for model parameters and pre-stresses. Reprinted by permission from Springer: Computer Methods in Biomechanics and Biomedical Engineering. Lecture Notes in Bioengineering, Gefen A., Weihs D., 2018

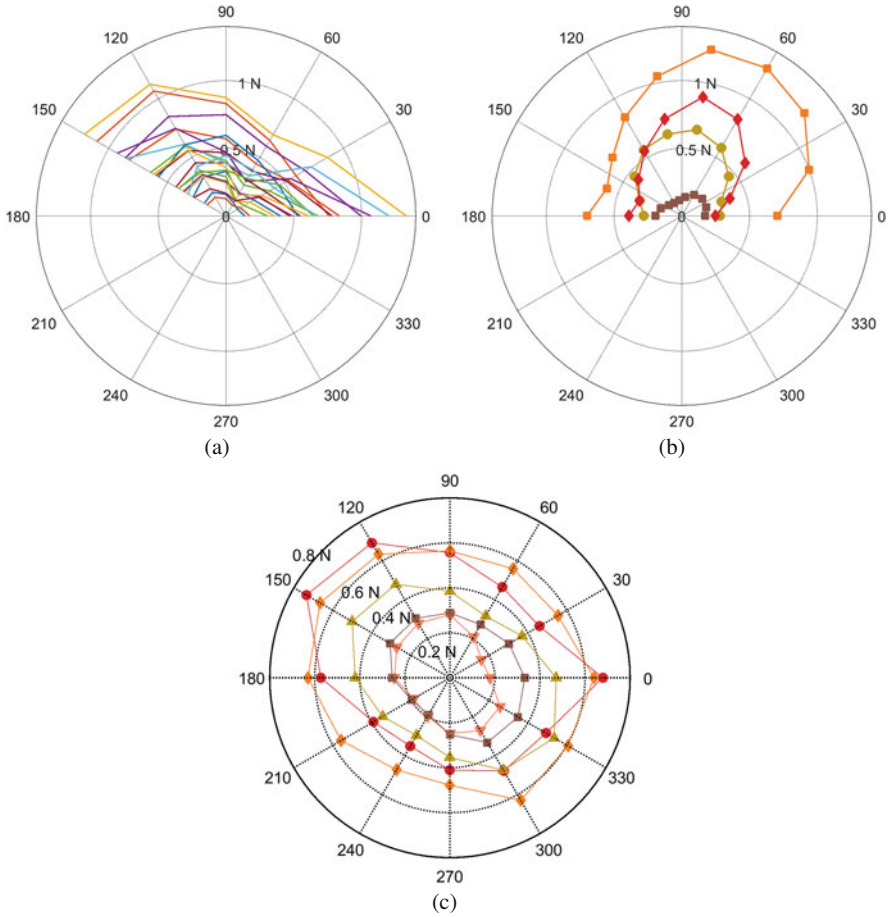

Fig. 8 In-plane force reaction for different directions for volunteers at (**a**) 0.9 mm displacement for anterior forearm; (**b**) 1.3 mm displacement for upper arm; (**c**) 1.1 mm displacement for central cheek. Note that forearm data was recorded up to 150° and upper arm data was recorded up to 180°. 0° is in the direction of the X-axis, which is defined for each location in Fig. 4. (c) Reprinted from Journal of the Mechanical Behavior of Biomedical Materials, 28, Cormac Flynn, Andrew J. Taberner, Poul M. F. Nielsen, and Sidney Fels, Simulating the three-dimensional deformation of in vivo facial skin, 484-494, 2013, with permission from Elsevier

response with similar VAFs. Both models simulated the response of the upper arm with a VAF of 98%.

The Ogden [32] model simulated the response of the facial skin with VAFs ranging from 93% to 96% (Table 2). The Bischoff et al. [4] and Ateshian and Costa [2] models simulated the response with similar agreements. The Gasser et al. [17] model had the smallest VAF (79%) when used to simulate forehead skin (Table 2). As a result, it was not used to simulate other regions of the face.

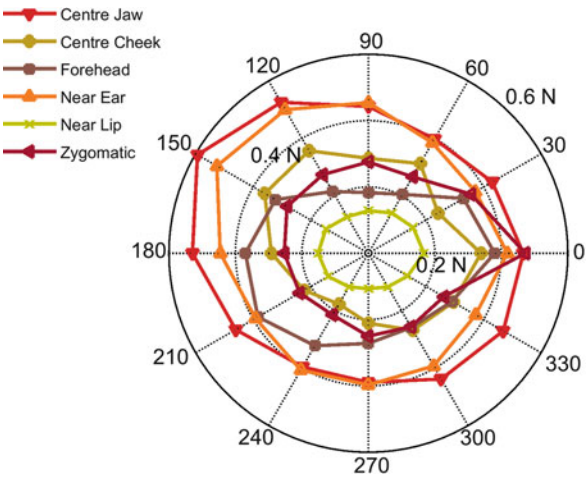

Fig. 9 In-plane force reaction at 0.7 mm displacement for different locations on one volunteer's face

3 Current Challenges and Future Directions

This chapter presented a method of characterising the mechanical response of in vivo human skin by applying a rich set of deformations using a micro-robotic device. The resulting force-displacement response from different points of the arm and face of volunteers exhibited non-linearity, anisotropy, and viscoelasticity. Qualitatively, the response of each volunteer's skin was similar. The direction of stiffest response corresponded, in general, to the direction of relaxed skin tension lines (RSTLs) in that area [5]. This in agreement with [34] in the central cheek region. However, the magnitude of the stiffness varied significantly according to volunteer [11]. This highlights the importance of getting patient-specific data for developing volunteer-specific models.

Using finite element analyses and non-linear optimisation, parameter sets were identified that best-fit the model responses to the experimental responses of different skin locations and different volunteers. VAFs ranging from 92% to 99 % were achieved for all the constitutive models tested except the Gasser et al. [17] model, which only achieved a VAF of 79% for the forehead region. The force-displacement response was too linear using this model. Overall, the anisotropic constitutive models did not perform better compared to the isotropic Ogden [32] model. Better knowledge of the structural characteristics of the skin through appropriate imaging in each case may guide the selection of anisotropic parameter values.

The optimisation procedure also estimated the in-vivo pre-stresses at the different locations. The pre-stresses ranged from 5 to 92 kPa, which is greater than values reported in the literature [9, 10, 21]. While this difference may be attributed to variations between individuals, it can also be due to the protocol used. Flynn et al. [12] demonstrated the importance of using out-of-plane deformations to estimate pre-stresses in skin. The normal response of skin is more dependent on the pre-stress than on the material parameters. With an application to cerebral aneursyms,

Table 1 Identified arm region material parameters, in vivo pre-stress field, and variance accounted for (*VAF*)

Region	Model	Model parameters	(σ_x, σ_y) (kPa)	*VAF* (%)
Anterior forearm (stiff)	Ogden [32]	$\mu_1 = 29.16$ kPa; $\mu_2 = 2.15$ Pa; $\alpha_1 = 1.71$; $\alpha_2 = 40.09$	(84, 61)	98
Anterior forearm (stiff)	Tong and Fung [40]	$c = 0.0107$ Pa; $A_1 = 40.636$; $A_2 = 21.837$; $a_1 = 12.754$ kPa; $a_2 = 6.057$ Pa; $a_3 = 38.046$ kPa	(92, 49)	99
Anterior forearm (medium)	Ogden [32]	$\mu_1 = 19.40$ kPa; $\mu_2 = 0.03$ Pa; $\alpha_1 = 1.00$; $\alpha_2 = 54.02$	(48, 39)	97
Anterior forearm (medium)	Tong and Fung [40]	$c = 0.0207$ Pa; $A_1 = 34.167$; $A_2 = 54.740$; $a_1 = 19.676$ kPa; $a_2 = 0.008$ Pa; $a_3 = 53.306$ kPa	(51, 31)	98
Anterior forearm (supple)	Ogden [32]	$\mu_1 = 10.06$ kPa; $\mu_2 = 0.001$ Pa; $\alpha_1 = 1.43$; $\alpha_2 = 37.62$	(39, 28)	98
Anterior forearm (supple)	Tong and Fung [40]	$c = 0.0221$ Pa; $A_1 = 26.772$; $A_2 = 40.846$; $a_1 = 20.956$ kPa; $a_2 = 0.390$ Pa; $a_3 = 31.675$ kPa	(38, 16)	98
Upper arm	Ogden [32]	$\mu_1 = 27.04$ kPa; $\mu_2 = 2.77$ Pa; $\alpha_1 = 3.79$; $\alpha_2 = 39.38$	(22, 48)	98
Upper arm	Tong and Fung [40]	$c = 0.1000$ Pa; $A_1 = 51.089$; $A_2 = 7.962$; $a_1 = 1.563$ kPa; $a_2 = 8772$ Pa; $a_3 = 12.355$ kPa	(17, 45)	98

The parameters are originally from Flynn et al. [12]. Reprinted by permission from Springer: Computer Methods in Biomechanics and Biomedical Engineering. Lecture Notes in Bioengineering, Gefen A., Weihs D., 2018

Lu et al. [29] showed that a normal load on a membrane structure can determine the wall tension without requiring accurate knowledge of the wall elastic properties. For the facial skin locations, some of the pre-stresses predicted using different constitutive models were similar. For example, using the Bischoff et al. [4] model the estimated pre-stress in the forehead region was 25 kPa, 23 kPa while using the Gasser et al. [17] model estimated the pre-stress in the same region to be 26 kPa, 18 kPa. The normal responses using both these models were similar to the experimental response [14]. In contrast, the Ateshian and Costa [2] model estimated a lower pre-stress of 7 kPa, 3 kPa for the forehead region but the predicted normal response was much lower than the experimental response. The pre-stress estimation may be improved by ensuring all the applied deformations have an out-of-plane component. The objective function would then have a greater weighting of out-of-plane responses.

Table 2 Identified facial region material parameters, in vivo pre-stress field, and variance accounted for (*VAF*)

Region	Model	Model parameters	(σ_x, σ_y) (kPa)	*VAF* (%)
Forehead	Bischoff et al. [4]	$n = 6.632 \times 10^{11}$ (mm^{-3}); $(a, b, c) =$ (0.8529, 1.272, 1.386)	(25, 23)	94
Forehead	Ateshian and Costa [2]	$c = 0.3118$ kPa; $\lambda_{11} = 0.9982$ kPa; $\lambda_{22} = 1.005$ kPa; $\mu_1 = 7.169$ kPa; $\mu_2 = 7.142$ kPa	(7, 3)	94
Forehead	Gasser et al. [17]	$\mu = 14.08$ kPa; $k_1 = 11.01$ kPa; $k_2 = 0.09188$; $\theta = 30.82^o$	(26, 18)	79
Forehead	Ogden [32]	$\mu_1 = 53.95$ kPa; $\mu_2 = 0.3012$ Pa; $\alpha_1 = 1.868$; $\alpha_2 = 69.00$	(34, 27)	94
Near lip	Bischoff et al. [4]	$n = 5.690 \times 10^{11}$ (mm^{-3}); $(a, b, c) =$ (0.6952, 1.276, 1.529)	(9, 8)	94
Near lip	Ateshian and Costa [2]	$c = 0.3291$ kPa; $\lambda_{11} = 1.0$ kPa; $\lambda_{22} = 6.387$ kPa; $\mu_1 = 4.556$ kPa; $\mu_2 = 2.352$ kPa	(9, 7)	91
Near lip	Ogden [32]	$\mu_1 = 41.29$ kPa; $\mu_2 = 0.16$ Pa; $\alpha_1 = 1.658$; $\alpha_2 = 54.964$	(24, 16)	93
Central cheek	Bischoff et al. [4]	$n = 1.246 \times 10^{12}$ (mm^{-3}); $(a, b, c) =$ (0.7880, 1.246, 1.446)	(53, 46)	92
Central cheek	Ateshian and Costa [2]	$c = 0.4421$ kPa; $\lambda_{11} = 1.0$ kPa; $\lambda_{22} = 1.0$ kPa; $\mu_1 = 6.121$ kPa; $\mu_2 = 4.353$ kPa	(10, 5)	93
Central cheek	Ogden [32]	$\mu_1 = 58.27$ kPa; $\mu_2 = 0.14$ Pa; $\alpha_1 = 2.334$; $\alpha_2 = 33.081$	(89, 72)	93
Central jaw	Bischoff et al. [4]	$n = 8.922 \times 10^{11}$ (mm^{-3}); $(a, b, c) =$ (0.8406, 1.224, 1.413)	(37, 32)	96
Central jaw	Ateshian and Costa [2]	$c = 0.5010$ kPa; $\lambda_{11} = 1.000$ kPa; $\lambda_{22} = 1.000$ kPa; $\mu_1 = 3.322$ kPa; $\mu_2 = 5.919$ kPa	(20, 16)	95
Central jaw	Ogden [32]	$\mu_1 = 57.73$ kPa; $\mu_2 = 0.42$ Pa; $\alpha_1 = 2.265$; $\alpha_2 = 34.689$	(81, 75)	96

The parameters are originally from Flynn et al. [13] and Flynn et al. [14]. Reprinted by permission from Springer: Computer Methods in Biomechanics and Biomedical Engineering. Lecture Notes in Bioengineering, Gefen A., Weihs D., 2018

The uniqueness of the parameter sets needs to be established. For simple uniaxial and biaxial tests on natural rubber, it is possible to identify several optimum parameter sets that result in the same quality of fit of model data to experimental data [33]. Using a richer set of deformations as was done for the arm and facial skin studies increases the identifiability of the material parameters and pre-

stresses. Flynn et al. [12] demonstrated improved identifiability when out-of-plane deformations were applied to the skin. This could be improved by enriching the data set further by tracking the displacement of the skin around the probe using DIC.

There are several opportunities to improve the finite element model used to simulate the experiments. For all the locations, the skin surface was assumed to be flat and underlying layers and connections were ignored. This assumption is weak in certain areas such as the zygomatic region of the face, whose surface is curved and is also the location of the zygomatic ligament, which anchors the facial skin to the underlying bone [16]. It is likely with probe displacements of 1.2–1.4 mm and an assumed skin thickness of 1.5 mm that the underlying layers of the skin would influence the force response. The influence of the underlying connections also may explain why the in-plane force in diametrically opposed directions differ (e.g. 330° and 150° in Fig. 8c). If there were no underlying connections, the response would be expected to be the same. Including the sub-dermal layers and ligaments is likely to improve the normal response of the skin. In general, the model simulated the response of arm skin (97–99%) better than the response of facial skin (91–96%). This could be attributed to the model assumptions being more realistic for arm skin than for facial skin.

The quasi-static loading of the skin surface is limiting in terms of full mechanical characterisation. Recently, Parker et al. [35] have used a revised version of the micro-robot to characterise the dynamic response of skin of the anterior forearm and hand using nonlinear stochastic system identification methods. Chen and Hunter [6] also used stochastic identification techniques with a dynamic indenter that needed to be reconfigured for each applied load direction.

The experimental protocol using the micro-robot and support plate is time consuming and sometimes uncomfortable for the volunteer. This is particularly true when testing facial skin. It is unlikely that this approach would be suitable for use in a clinical context where the comfort of the patient is important. Hand-held devices such as that proposed by HajiRassouliha et al. [19], which measures three-dimensional strain fields of skin, are likely to point the way forward to accessible characterisation of a patient's skin in the clinic.

References

1. Affagard J-S, Wijanto F, Allain J-M (2017) Improving the experimental protocol for a more accurate identification of a given mechanical behaviour in a single assay: Application to skin. Strain 53(5):e12236
2. Ateshian GA, Costa KD (2009) A frame-invariant formulation of Fung elasticity. J Biomech 42(6):781–785
3. Bischoff JE, Arruda EM, Grosh K (2000) Finite element modeling of human skin using an isotropic, nonlinear elastic constitutive model. J Biomech 33(6):645–652
4. Bischoff JE, Arruda EA, Grosh K (2002) A microstructurally based orthotropic hyperelastic constitutive law. J Appl Mech Trans ASME 69(5):570–579
5. Borges AF (1989) Relaxed skin tension lines. Dermatol Clin 7(1):169–177

6. Chen Y, Hunter IW (2009) In vivo characterization of skin using a weiner nonlinear stochastic system identification method. Conf Proc IEEE Eng Med Biol Soc 2009:6010–6013
7. Coutts LV, Miller NR, Mortimer PS, Bamber JC (2016) Investigation of In Vivo skin stiffness anisotropy in breast cancer related lymphoedema. J Biomech 49(1), 94–99
8. Cowley K, Vanoosthuyze K (2016) The biomechanics of blade shaving. Int J Cosmet Sci 38(S1):17–23
9. de Jong LAM (1995) Pre-tension and anisotropy in skin: modelling and experiments
10. Diridollou S, Patat F, Gens F, Vaillant L, Black D, Lagarde JM, Gall Y, Berson M (2000) In vivo model of the mechanical properties of the human skin under suction. Skin Res Technol 6(4):214–221
11. Evans SL, Holt CA (2009) Measuring the mechanical properties of human skin in vivo using digital image correlation and finite element modelling J Strain Anal Eng Des 44(5):337–345
12. Flynn C, Taberner A, Nielsen P (2011) Modeling the mechanical response of in vivo human skin under a rich set of deformations. Ann Biomed Eng 39(7):1935–1946
13. Flynn C, Taberner AJ, Nielsen PMF, Fels S (2013) Simulating the three-dimensional deformation of in vivo facial skin. J Mech Behav Biomed Mater 28:484–494
14. Flynn C, Taberner AT, Fels S, Nielsen PMF (2018) Comparison of anisotropic models to simulate the mechanical response of facial skin. In: Computer methods in biomechanics and biomedical engineering. Springer, NewYork, pp 43–55
15. Fung YC (1993) Biomechanics: mechanical properties of living tissues. Springer, New York
16. Furnas DW (1989) The retaining ligaments of the cheek. Plast Reconstr Surg 83(1):11–16
17. Gasser TC, Ogden RW, Holzapfel GA (2006) Hyperelastic modelling of arterial layers with distributed collagen fibre orientations. J R Soc Interface 3(6), 15–35
18. Ha RY, Nojima K, Adams WP, Brown SA (2005) Analysis of facial skin thickness: defining the relative thickness index. Plast Reconstr Surg 115(6):1769–1773
19. HajiRassouliha A, Kmiecik B, Taberner AJ, Nash MP, Nielsen PMF (2015) A low-cost, hand-held stereoscopic device for measuring dynamic deformations of skin in vivo. In: 2015 international conference on Image and Vision Computing New Zealand (IVCNZ) IEEE, New York, pp 1–6
20. Hsu C-C, Tsai W-C, Hsiao T-Y, Tseng F-Y, Shau Y-W, Wang C-L, Lin S-C (2009) Diabetic effects on microchambers and macrochambers tissue properties in human heel pads. Clin Biomech 24(8):682–686
21. Jacquet E, Josse G, Khatyr F, Garcin C (2008) A new experimental method for measuring skin's natural tension. Skin Res Technol 14(1):1–7
22. Jin X, Zhu DD, Chen BZ, Ashfaq M, Guo XD (2018) Insulin delivery systems combined with microneedle technology. Adv Drug Delivery Rev 127:119–137
23. Jor J, Nash M, Nielsen P, Hunter P (2011) Estimating material parameters of a structurally based constitutive relation for skin mechanics. Biomech Model Mechanobiol 10(5):767–778
24. Karwoski AC, Plaut RH (2004) Experiments on peeling adhesive tapes from human forearms. Skin Res Technol 10(4):271–277
25. Kelly R, Watts L (2017) Slow but likeable? Inefficient robots as caring team members. Robots in Groups and Teams, p 1
26. Killaars RC, Lopez Penha TR, Heuts EM, van der Hulst RRJW, Piatkowski AA (2015) Biomechanical properties of the skin in patients with breast cancer-related lymphedema compared to healthy individuals. Lymphat Res Biol 13(3):215–221
27. Kvistedal YA, Nielsen PMF (2009) Estimating material parameters of human skin in vivo. Biomech Model Mechanobiol 8(1):1–8
28. Liu L, Kuffel K, Scott DK, Constantinescu G, Chung H-J, Rieger J (2017) Silicone-based adhesives for long-term skin application: cleaning protocols and their effect on peel strength. Biomed Phys Eng Express 4(1):015004
29. Lu J, Zhou X, Raghavan ML (2008) Inverse method of stress analysis for cerebral aneurysms. Biomech Model Mechanobiol 7(6):477–486
30. Maas SA, Ellis BJ, Ateshian GA, Weiss JA (2012) FEBio: finite elements for biomechanics. J Biomech Eng 134(1):011005

31. Mori M, MacDorman KF, Kageki N (2012) The uncanny valley [from the field]. IEEE Robot Autom Mag 19(2):98–100
32. Ogden RW (1972) Large deformation isotropic elasticity - on the correlation of theory and experiment for incompressible rubberlike solids. Proc R Soc Lond A Math Phys Sci 326(1567):565–584
33. Ogden RW, Saccomandi G, Sgura I (2004) Fitting hyperelastic models to experimental data. Comput Mech 34(6):484–502
34. Ohshima H, Tada A, Kanamaru A, Akamatsu H, Sakai Y, Itoh M, Kanto H (2011) Relevance of the directionality of skin elasticity to aging and sagging of the face. Skin Res Technol 17(1):101–107
35. Parker MD, Jones LA, Hunter IW, Taberner AJ, Nash MP, Nielsen PMF (2017) Multidirectional in vivo characterization of skin using Wiener nonlinear stochastic system identification techniques. J Biomech Eng 139(1):011004
36. Reihsner R, Balogh B, Menzel EJ (1995) Two-dimensional elastic properties of human skin in terms of an incremental model at the in vivo configuration. Med Eng Phys 17(4):304–313
37. Sagar M, Bullivant D, Robertson P, Efimov O, Jawed K, Kalarot R, Wu T (2014) A neurobehavioural framework for autonomous animation of virtual human faces. In: SIGGRAPH Asia 2014 autonomous virtual humans and social robot for telepresence. ACM, New York, p. 2
38. Tepole AB, Gart M, Gosain AK, Kuhl E (2014) Characterization of living skin using multiview stereo and isogeometric analysis. Acta Biomater 10(11), 4822–4831
39. Then C, Stassen B, Depta K, Silber G (2017) New methodology for mechanical characterization of human superficial facial tissue anisotropic behaviour in vivo. J Mech Behav Biomed Mater 71:68–79
40. Tong P, Fung Y-C (1976) The stress-strain relationship for the skin. J Biomech 9(10):649–657
41. Tonge TK, Atlan LS, Voo LM, Nguyen TD (2013) Full-field bulge test for planar anisotropic tissues: part I - experimental methods applied to human skin tissue. Acta Biomater 9(4):5913–5925
42. Trowbridge MM, Wang B, Gutshall D, Rodenberg CA, Farage MA (2017) A randomized, controlled trial comparing skin health effects and comfort of two adult incontinence protective underwear. Skin Res Technol 23(2):202–211